*applied sciences*

MDPI

*Article*

# Development of a Leak Detection System Based on Fiber Optic DTS Monitoring and Validation on a Full-Scale Model

**Diego Antolín-Cañada [1,*], Pedro Luis Lopez-Julian [2], Javier Pérez [2], Óscar Muñoz [3], Alejandro Acero-Oliete [2] and Beniamino Russo [4]**

[1] Grupo de Electrónica de Potencia y Microelectrónica (GEPM), Escuela Universitaria Politécnica de la Almunia (EUPLA), Universidad de Zaragoza, 50009 Zaragoza, Spain
[2] Grupo de Ingeniería Hidráulica y Ambiental (GIHA), Escuela Universitaria Politécnica de La Almunia (EUPLA), La Almunia, 50100 Zaragoza, Spain; pllopez@unizar.es (P.L.L.-J.); jpereze@unizar.es (J.P.); acero@unizar.es (A.A.-O.)
[3] Smart Systems, Tecnalia, Basque Research and Technology Alliance (BRTA), 20009 Donostia-San Sebastian, Spain; oscar.munoz@tecnalia.com
[4] Flumen Research Institute, Universitat Politècnica de Catalunya, BarcelonaTech (UPC), Centre Internacional de Mètodes Numèrics a l'Enginyeria (CIMNE), Campus Nord, 080043 Barcelona, Spain; beniamino.russo@upc.edu
* Correspondence: dantolin@unizar.es

## Featured Application

Leak detection in ponds that store liquids, for example irrigation water ponds, or slurry ponds in the swine sector.

## Abstract

Leaks in ponds are a problem due to the loss of water resources, although the problem is greater when the ponds store livestock or agricultural waste (slurry or wastewater), in which case there is a risk of hydrogeological contamination of the environment. The proposed leak detection system is based on distributed temperature sensing (DTS) with hybrid fiber optics using the Raman effect. Using active detection techniques, i.e., applying a specific amount of electrical power to the copper wires that form part of the hybrid cable, it is possible to increase the temperature along the fiber and measure the thermal increments along it, detecting and locating the point of leakage. To validate the system, a full-scale prototype reservoir (25 m × 10 m × 3.5 m) was built, equipped with mechanisms to simulate leaks under the impermeable sheet that retains the reservoir's contents. For environmental reasons, the tests were carried out with clean water. The results of the leak simulation showed significant differences in temperature increases due to the electrical pulse in the areas affected by the simulated leak (1 °C increase) and the areas not affected (5 °C increase). This technology, which uses hybrid fiber optics and a low-cost sensor, can be applied not only to ponds, but also to other types of infrastructure that store or retain liquids, such as dams, where it has already been tested, to measure groundwater flow, etc.

**Keywords:** DTS sensor; leak detector; leak detector in ponds; DTS detection system



Academic Editors: Bruno Brunone, Seungseop Jin and Wongi S. Na

Received: 17 November 2025
Revised: 30 December 2025
Accepted: 31 December 2025
Published: 1 January 2026



## 1. Introduction

Ponds are storage infrastructures in the agricultural sector and can be designed both to contain water for irrigation and to accumulate water for livestock farms. In both cases, losses of the stored water are very frequent and, for the case of irrigation installation, can

imply a significant reduction in terms of available resources. On the other hand, in the case of livestock waste ponds, losses and their consequent infiltration into the subsoil constitute a clear risk of contamination of the ground and surface water environment, slurry being an obvious example.

This work is part of the Digit-Balsa project as a pilot test for the detection of leaks in slurry ponds, the system was launched in the spring of 2023. The validation tests on the leak detection system have been carried out using water as a loss effect, for two reasons. The first one is the contamination of water resources for possible irrigation and drinking water when producing a slurry leak, and the second one is due to the fact that in the literature, the systems that use this technology do it for the detection of water flow.

Within the agricultural sector, leak detection systems in irrigation ponds are important to avoid leaks in the ponds due to deterioration of the impermeable sheet that retains water, as an environmental safety measure.

In the specific case of ponds intended to store slurry, the European normative reference document on best available techniques to be applied for intensive pig and poultry farming [1] established the need to annually check the structural integrity of existing slurry ponds, given that they did not have the leak detection systems already required for newly constructed ones.

For these reasons, the early detection of leaks of liquids stored in a pond, as well as the location of the leakage point with certain precision, is a field of obvious interest in the maintenance and control of water infrastructures, both from an economic and environmental perspective, bringing the agricultural and livestock sectors.

Traditionally, leaks in slurry ponds are detected by visual inspection, identifying a leak when liquid flows from the drainage pipes. Although this technique does not allow for leak location or early detection, the speed of detection depends on the size of the leak—the larger the leak, the less time it will take for liquid to flow out of the drainage pipes—as well as on periodic visual inspection.

One technique for monitoring hydraulic infrastructure that allows distributed temperature measurement using a fiber optic (FO) system is the use of Fiber Bragg Grating (FBG), although this technology requires a sensor for each temperature measurement point, rapidly increasing the cost of deployment as the number of measurement points increases.

Another Distributed Temperature Sensor (DTS) measurement technique is the use of hybrid fiber optics based on Raman effect temperature measurement. In this technology, the hybrid fiber optic is the sensor itself, allowing temperature measurement along its length with a linear resolution that depends on the Raman interrogator used. The fact that the optical fiber is the distributed sensor reduces the cost of the system. Given that the target application is in the livestock and agricultural sectors, the cost of the system must be reduced so as not to increase the price of food products.

Given the characteristics of a pond, a low-cost distributed measurement system is required to detect leaks over long distances in the subsoil. For a monitoring system with these characteristics, the use of hybrid fiber optics as a DTS is a suitable solution [2]. The use of fiber optics has been applied in different types of hydraulic works with the aim of qualitatively and quantitatively detecting possible water seepage [3–5]. Hybrid cables consist of one or more fiber optic cables and one or more copper cables, all within the same insulation, allowing not only to perform temperature measurements, but also to supply the thermal pulse to analyze the behavior of the ground around the buried fiber along the entire monitored length.

Within the systems based on the measurement of distributed temperature with optical fiber to detect water flows, we can find mainly two types, passive and active. Passive systems do not intentionally or actively modify the operating conditions of the fiber by

taking the distributed temperature measurement of the environment as it is. The specific characteristics of each type of work require a prior definition of the measurement conditions, adapted to each particular situation [6].

Due to the cost of implementing the systems in man-made hydraulic infrastructures, it is common to develop laboratory systems either in controlled environments, such as those presented in [7,8] which shows a scale simulation of levee seepage, or the previous laboratory work that precedes the present work [9] where a leakage from a controlled impermeable sheet is simulated.

In these types of systems, different detection mechanisms have been reported in [10]. In the analysis of a leak detection system through distributed temperature measurement with optical fiber, we will focus on two, the passive method, i.e., without heating the hybrid cable, and the active method with heating. In both cases, the applications that can be found are very similar.

First, we will review the detection systems by passive methods, which are based on the measurement of the temperature distributed along the cable over time. Subsequently, an analysis is made of the data collected and the differences shown with respect to the same time of the year, as well as nearby points of the fiber.

Within the systems, we find different fiber distributions, either transversally detecting temperature variations according to the depth of penetration of the cable or longitudinally along a linear work.

In this first case, refs. [11–13] have been found, where the researchers are studying the behavior of the civil work of canalization of the Adige river, close to a highway, with distributed optical fiber sensors (DFOSs).

On the other hand, we found systems that heat the fiber as a perturbation medium for detecting water flows. These systems have a higher detection accuracy, at the cost of the energy consumption to heat the fiber through the copper wires that are part of the hybrid cable. Given the a priori higher resolution of detection and the relatively small water flow that can be produced by a leak in an irrigation or slurry pond, this last system will be used in this project.

In [14], the authors present a system for monitoring temperature and detecting groundwater discharge under a river. In this case of active detection, hybrid fiber cables are deployed in deep boreholes perpendicular to the earth's surface for detection [11–13].

Other authors propose the combination of passive and active sensing systems such as [15,16]. The former combines passive and active measures to locate and quantify the variability of groundwater discharge in a stream, while the latter uses it as a downhole tool in hydrogeology. With this same combination in [17], they use this technique to estimate infiltration rates in a managed aquifer recharge framework.

With a use more similar to the one related to this project in [5,18] a real-time dam leak detection system has been found with an FO cable distribution along the dam line. This technology is applied as a complement to conventional sensors used in dam monitoring systems, and this new technique avoids problems due to point measurements and late detection that often occurs when the processes of slope instability or seepage in the body of the dam are already too advanced, with significant environmental impacts and potential risk of irreversible deterioration of the infrastructure.

Passive methods have the advantage of not requiring a cable heating system, although they do require a high-precision integrator, as the thermal variations to be detected are between 0.1 and 0.5 °C. In addition, precise calibration of the interrogator is necessary. However, active methods detect thermal variations above one degree Celsius, which requires less precision in measurement and provides greater reliability in detection.

Following the tests carried out on the laboratory model, which were presented in [9] and which proved to be satisfactory but on a limited scale, this paper proceeds to the design and construction of a full-scale model with the aim of validating the methodology on a full scale.

The paper is structured as follows: Section 2 provides a description of the infrastructure developed for the full-scale model of the leak detection system in ponds. Section 3 presents the results of the measurements in different tests performed. Section 4 compares the results obtained in this study with the results obtained in other types of applications. Finally, Section 5 presents the conclusions of the work.

## 2. Materials and Methods

The first subsection of this section explains the location of the constructed pond. In the following subsection, we study the constructive development, including the construction plans of the civil works and the installation and distribution of the optical fiber. Finally, the third section describes the active DTS measurement system with the necessary instrumentation for monitoring leaks in the basin.

### *2.1. Ponds Location*

The reservoir is located in the town of La Almunia de Doña Godina, Spain, at the geographical coordinates 41°29′22.1″ N–1°23′36.1″ W.

At present, due to environmental considerations, the pond is intended for clean water storage as simulations of losses of the stored content are to be carried out. However, in constructive terms, the project has been executed as if it were to be filled with slurry, complying with the applicable regulations for the operation of this type of pond.

Tertiary materials identified as "calcareous crusts" according to the Geological Map of Spain (sheet 410, La Almunia de Doña Godina) outcrop on the plot where the reservoir is to be built. Figure 1 shows the area of the geological map, at a scale of 1:50,000, where the planned reservoir is located.

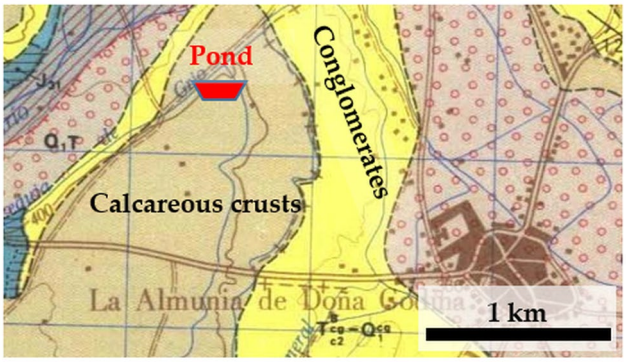


**Figure 1.** Location of the pond projected on the geological map at scale 1:50,000.

The substratum of this entire geographical area is made up of tertiary materials that are geotechnically of the coarse-grained soil type, appearing partially cemented, giving rise to calcareous crusts of sub-metric thickness.

### *2.2. Ponds Construction, Fiber Deployment, and Leakage Simulation System Design*

The most realistic method to simulate a leak would be to create a controlled rupture in the waterproofing sheet. However, this approach presents significant difficulties: each simulation would require rupturing a new area, emptying the basin, repairing the sheet, and refilling the reservoir. This process would have a very high cost both in time between

simulations and in the consumption of water resources in the filling and emptying of the pond.

The proposed solution is to introduce under the pond, buried under the geotextile that protects the impermeable layer of the soil, and a set of PVC pipes controlled by valves and connected to a pump.

The design of the basin, together with the fiber distribution and the leakage simulation system, must be carried out in combination prior to the construction of the basin. The pond has been constructed in accordance with the standard for slurry storage ponds.

Figure 2 shows the plan drawing of the construction design of the prototype basin. In the center of the plan, the bottom drains, which will collect the water from the leaks, can be seen in purple. In dashed pink, the distribution of the hybrid fiber is shown. It leaves the control house towards the upper slope of the image, going to the leftmost slope where it turns at a lower level closer to the bottom of the basin and returns parallel to the inlet fiber line at the same level. When it reaches the left-hand slope, it turns towards the base and runs parallel to the first of the drains. It is carried to the other end of the raft base parallel to the drain and turned again to return parallel to the drain. In this way, the fiber is distributed parallel on both sides of the drain.

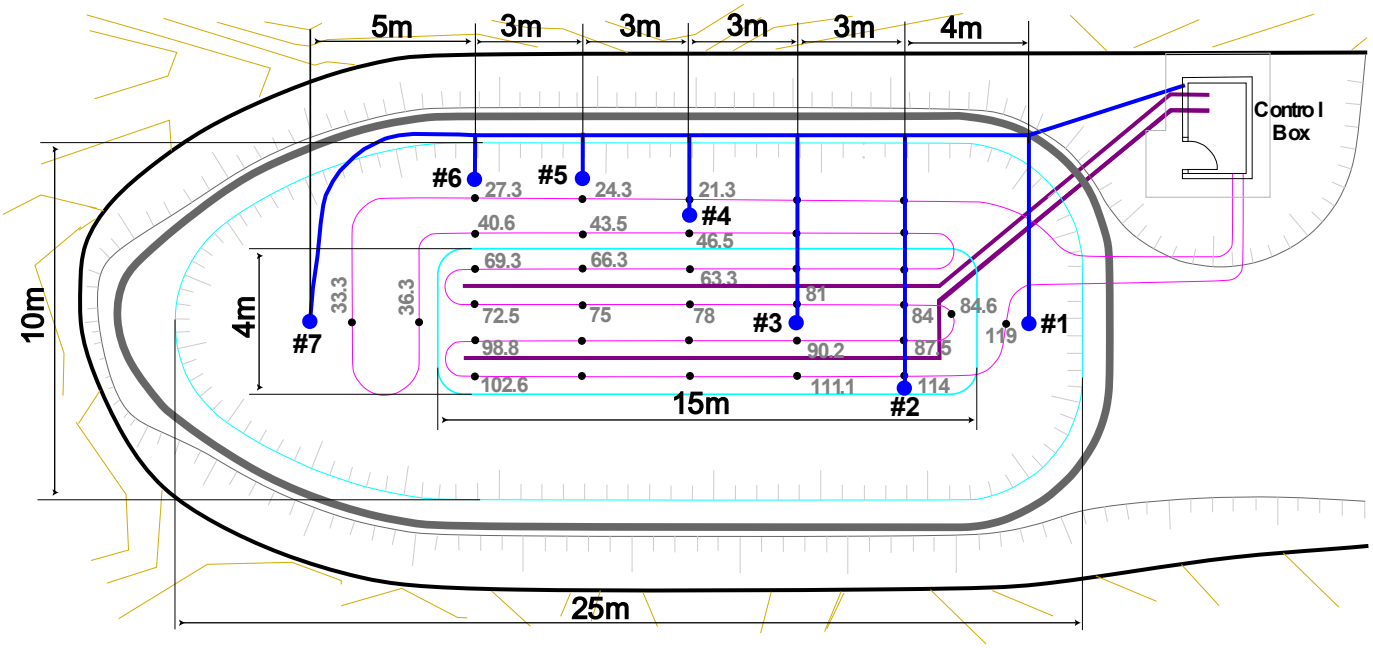


**Figure 2.** Floor plan of the pond. The dark blue lines represent the pipes simulating leaks found under the geotextile fiber and on the ground. The pink lines show the layout of the hybrid fiber optic cable on the upper slope of the image and at the base of the pond. The purple lines are the dredging pipes. The cyan lines correspond to the outline of the pond on the outside and the flat base of the pond on the inside of the image. The black numbers are the identifiers of the pipes where the leak point is located, and the gray numbers are the metric points of the fiber in meters. The valve number is abbreviated as # for the rest of the text.

The objective of this distribution is for the fiber to be able to detect leaks originating both on the slope and at the bottom of the reservoir.

Figure 3 shows the transverse section of the raft. At the bottom, the drains can be seen, where the fluids from possible leaks will be collected. Therefore, it is to be expected that in the event of a leak, the liquid will flow into them. For this reason, the fiber has been distributed around the drains, and leak simulation taps have been installed close to them.

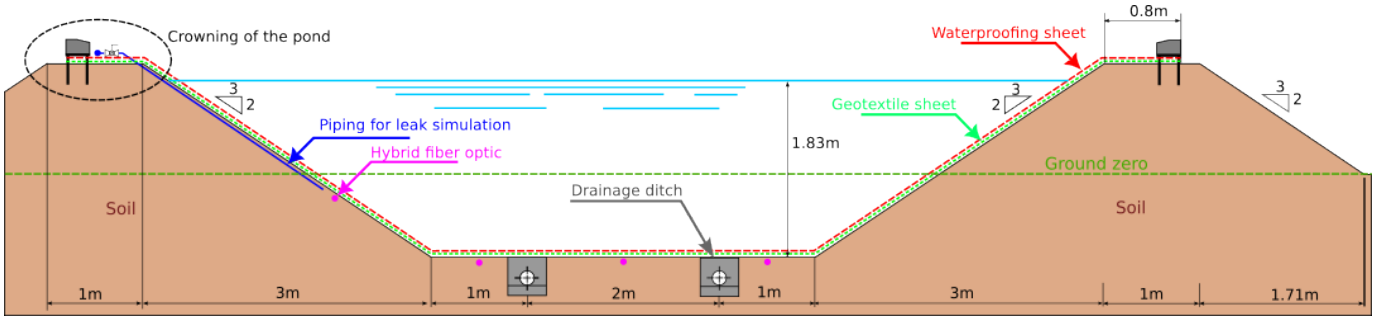


**Figure 3.** Transversal section of the basin.

On the other hand, leakage simulation taps have also been distributed in different parts of the basin slope, and the hybrid fiber has been distributed along the same slope. In this way, the aim is to check whether it is possible to detect leaks produced in the slope, the possibility of detecting the flow water towards the drains as it has to pass through the fiber at multiple points, and finally, to see whether the drains collect the possible leaks.

The pipes appear located in the detailed drawing of the basin in Figure 3, where they are marked in blue and are in different longitudinal and transverse positions in relation to both the drains and the distribution of the fiber optics, with the aim of being able to simulate as many situations as possible. The leakage simulation valve control system is located inside the control house and is shown in Figure 4.


**Figure 4.** Valves for leak simulation. The numbering of the valves is directly related to the representation of the leak points in Figure 2.

The leak simulation system is activated manually by operating the valves shown in Figure 4. These valves control the flow of water to the pipes located under the geotextile fiber and on the ground where the geotextile and geomembrane rest. Figures 2 and 3 show that there are seven pipes that simulate leaks at the points indicated in Figure 2, both on the slopes and at the base of the pond. The pipes are always located under the geotextile fiber so as not to damage the geomembrane and cause a real leak due to erosion.

Figure 5a,b show the deployment of the optical fiber under the bottom of the raft. While the images in Figure 5c,d show how the geotextile layer (white) is made on Polyethylene Terephthalate (PET) (GeoProtec SIS, Impermeabilizaciones Valcruz S.L., Valencia, Spain) that protects the waterproofing sheet (black) from possible erosion when it rubs against the soil. The waterproofing sheet, the geomembrane (Atarfil HD, Atarfil, Granada, Spain), is made on High-Density Polyethylene (HDPE) with 2 mm of thickness. The cable model

deployed is a Helucom A-DSQ(ZN)B2Y (Urkunde, Mendaro, Spain) with 4 Multimode G50/125 optic fiber cables with 4 copper wires inside.

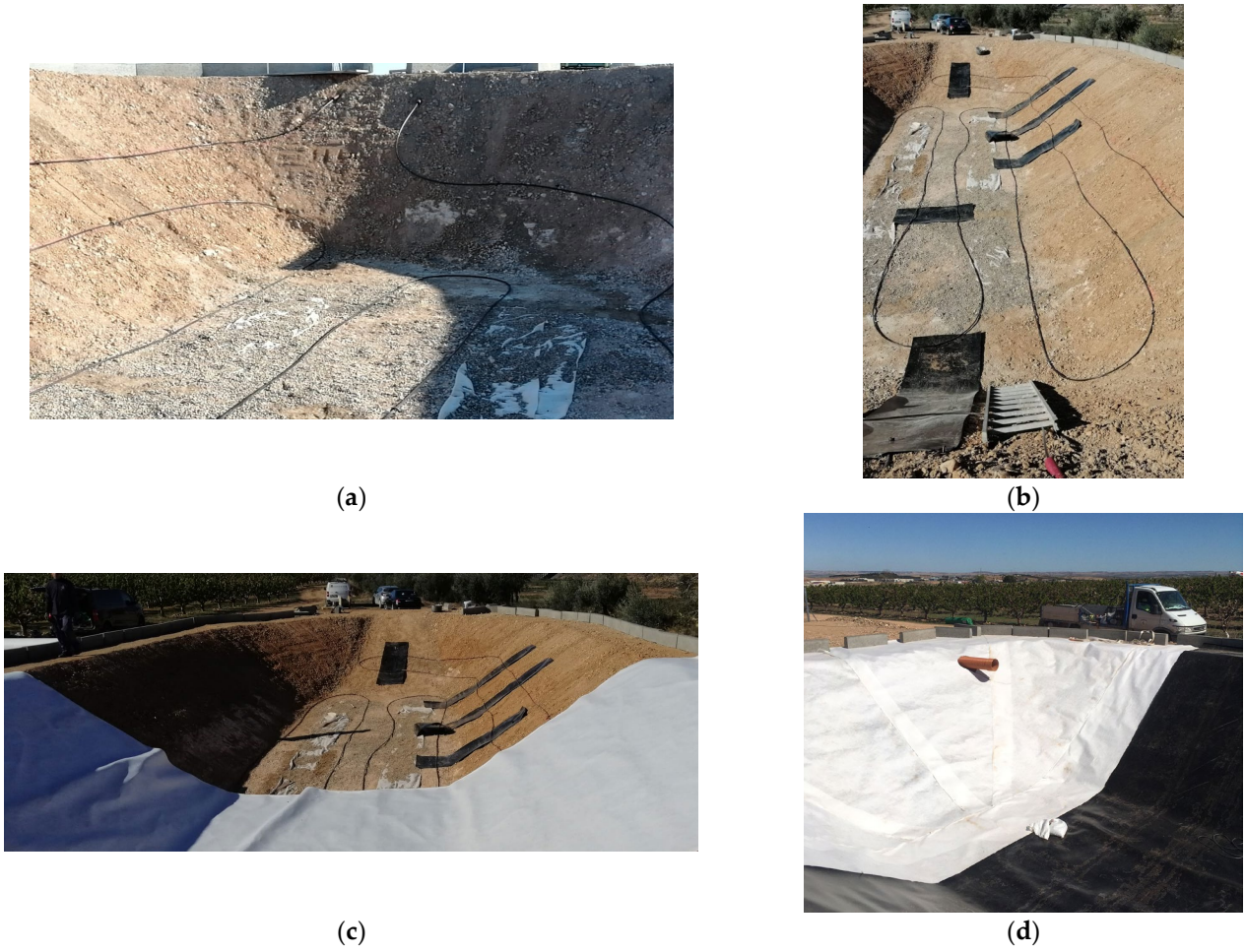

(**a**) (**b**) (**c**) (**d**)

**Figure 5.** Photographs of the construction process of the basin. (**a**) Installation of the fiber, detail of the entrance to the control house. (**b**) Preparation of the installation of the taps for the simulation of leaks. (**c**) Installation of the geotextile fiber. (**d**) Installation of the waterproofing layer on the geotextile fiber.

Finally, Figure 6 shows the constructed basin before filling with water.

**Figure 6.** Photograph of the raft just after its construction was completed and before its first filling.

### 2.3. Ponds Leakage Detection System Design

In the previous subsection, the construction of the basin, the full-scale model that will allow validation of the leak detection measurement system using DTS, was presented. In this section, the detection system itself, whose conceptual diagram is shown in Figure 7, will be presented.

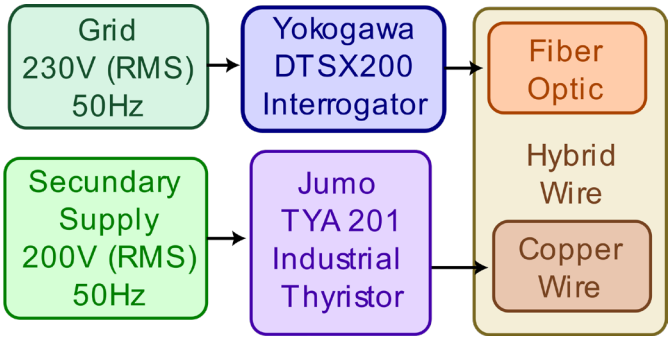


**Figure 7.** Schematic diagram of the detection system.

The diagram in Figure 7 shows two subsystems, the first one formed by the Yokogawa DTSX200 (Yokogawa Iberia, Madrid, Spain) interrogator, which is connected to the optical fiber and allows, by means of the RAMAN effect, to determine the fiber temperature with a thermal accuracy of 0.3 °C for a range of 1 km cable length and a spatial resolution that can vary at will from 1 m to 10 cm with a measurement periodicity of 1 min.

With the construction dimensions of the prototype basin in which 143 m of hybrid cable have been deployed (of which are buried under the basin, from meter 20 to meter 130), a resolution of 20 cm has been used, which will provide 550 instant and simultaneous measurements under the waterproof sheet.

Figure 8 shows the computer running the interrogator control software that allows the collection of temperature data at different points along the fiber.

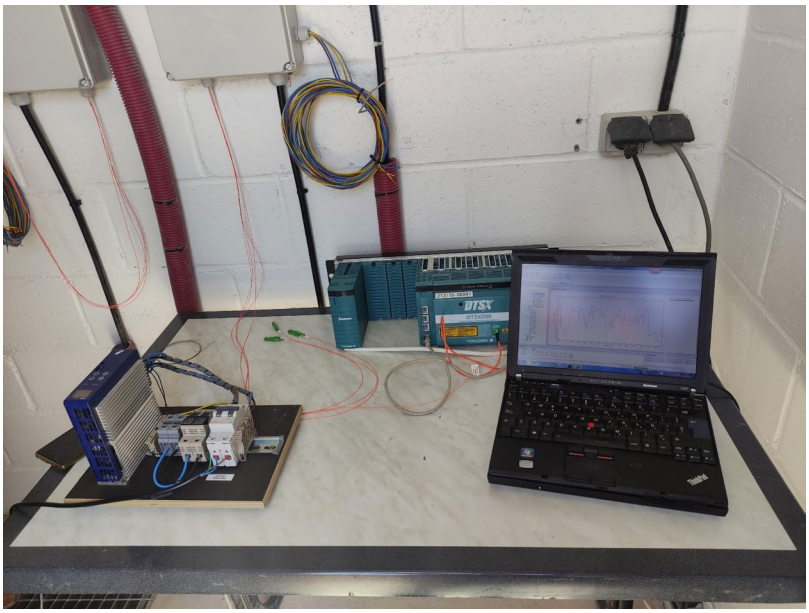

**Figure 8.** Photograph of the monitoring system (inside the control building).

The second subsystem enables fiber heating and comprises the active monitoring and detection system. For this, use is made of the resistance of the copper cables themselves

and an auxiliary resistor that reduces the peak current given the power supply available at the location of the raft.

At this location, the power supply system consists of photovoltaic panels, which are located on the roof of a building for the storage of tools and pumps filling a nearby farm.

The installation, in addition to the photovoltaic panels and their energy storage batteries, consists of an inverter that supplies a single-phase voltage of 230 V RMS as the main voltage. This power supply will be used to feed the interrogator and the control computer.

On the other hand, a secondary auxiliary power supply system has been used for the heating system, providing an output voltage of 200 V RMS, sufficient to power the Jumo TYA 201 (Jumo, Madrid, Spain) industrial thyristor that will control the power transmission in the cables. The power supply diagram is shown in Figure 9.

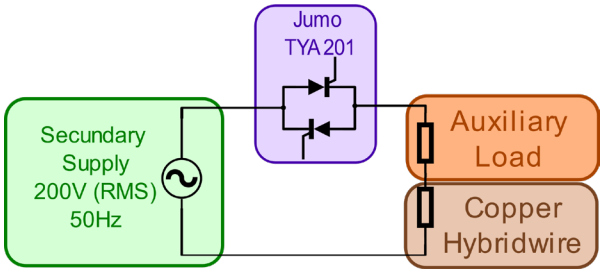


**Figure 9.** Electrical power supply diagram.

For an adequate detection, the power supplied by the heating system should be 10 W/m according to [19], while ref. [20] indicates that it should be between 30 and 40 W/m. In the system developed here, a power of 10 W/m has been adopted in order to reduce the electrical cost of the development, having proved to be sufficient to measure leakage in the present experimental conditions, according to the conclusions of [21], laboratory work whose conditions are similar to those verified in laboratory work prior to the one presented here [9].

Under these conditions, we proceed to calculate the theoretical resistance of the deployed cable, in order to subsequently be able to adjust its power. The cable resistance ($R$) is calculated by Equation (1):

$$R = \rho \cdot \frac{L}{A}, \tag{1}$$

where $\rho$ is the resistivity of copper ($1.68 \times 10^{-8}$ Ω·m), $L$ is the length of the cable, and $A$ is its cross-section.

In order to increase the resistance and take advantage of the four copper cables inside the hybrid fiber, these will be connected in series, so that the 143 linear meters deployed will become a total length of 572 m of copper with a section of 1.5 mm, according to the manufacturer. With these data, the resistance achieved is 5.44 Ω. An experimental measurement is made and its value provided is 7.77 Ω, and this difference may be due to the electrical resistance of the copper wire splices to obtain the length of 572 m.

The Jumo TYA 201 industrial thyristor is configured with an integral control so its peak current ($I_{peak}$) at 200 V root mean square (RMS) supply voltage ($V_{RMS}$) is given by Equation (2):

$$I_{Peak} = \frac{\sqrt{2} \cdot V_{RMS}}{R} = \frac{\sqrt{2} \cdot 200\ \text{V}}{7.77\ \Omega} = 36.4\ \text{A}. \tag{2}$$

This current value is very high, being outside the working capacity of the thyristors used, and being a very high value for a conventional single-phase electrical installation, so a resistive electrical load is installed in series with the hybrid cable whose experimental measurement provides a resistance of 18.27 Ω as a whole. With this resistance, applying

Equation (2), we obtain a peak current of 15.48 A. This value is already within the operating range of the thyristor and a more conventional electrical installation.

As the system presents a resistive load and has an integral control in the AC/AC conversion, the voltage of the load is represented in Figure 10 in a generic way.

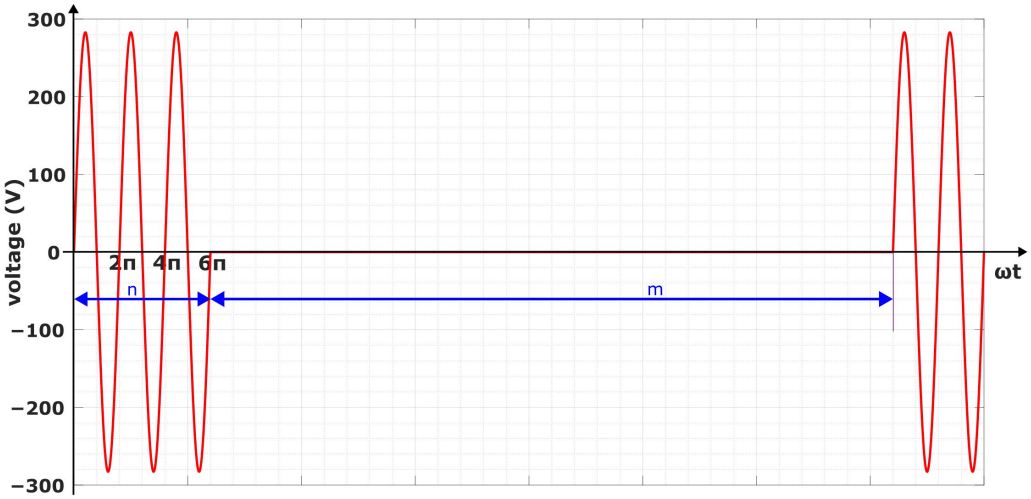


**Figure 10.** Output voltage waveform or at load with integral thyristor control.

In Figure 10, $n$ is the cycle number while $m$ is the number of signal cycles in which the thyristors remain in cutoff and no power is supplied to the load. The sum of the two is the number of cycles and thus the time period over which control is applied.

Applying the definition of voltage root mean square to the wave of Figure 10, we obtain the expression of Equation (3):

$$V_{ORMS} = \sqrt{\left[\frac{n}{2\pi(n+m)} \cdot \int_0^{2\pi} 2V_{GRMS}^2 \cdot \sin^2(\omega t) \cdot d(\omega t)\right]} = V_{GRMS} \cdot \sqrt{\frac{n}{n+m}}, \quad (3)$$

where $V_G$ is the supply voltage and $V_O$ the output voltage both values in root mean square (RMS). $V_O$ is the voltage supplied to the equivalent resistance of the hybrid cable. If, in this expression, we extract the relation between $n$ and $m$ as a constant $k$, shown in Equation (4)

$$k = \frac{n}{n+m}, \quad (4)$$

so that the expression for the RMS output voltage is as in Equation (5),

$$V_{ORMS} = V_{GRMS} \cdot \sqrt{k}, \quad (5)$$

applying 5 to the power calculation in the load, Equation (6) is obtained as follows:

$$P_O = \frac{V_{ORMS}^2}{R} = \frac{V_{GRMS}^2 \cdot k}{R} \quad (6)$$

where $P_O$ is the output power or power delivered to the equivalent resistance of the hybrid cable.

The Jumo thyristor is configured to perform a power control for a resistive load, so that when configured to work at 50% power, the $k$ factor of Equation (6) refers to the power level to be provided. In the test conditions $k$ = 0.5, so that the power provided to the load is 1065.5 W, divided by the number of meters of cable deployed, we obtain that in these conditions, the power delivered is 7.5 W/m, lower than the values of 10 W/m proposed in [19] and much lower than the 30–40 W/m proposed in [20]. As we will see later, this power level is sufficient to allow leak detection.

### 2.4. Description of the Test Methodology

Once the location and characteristics of the terrain where the raft is located, the construction and deployment of the fiber and, finally, the active heating system of the hybrid cable have been indicated, it only remains to describe the test methodology used.

The tests were carried out sequentially in different steps, each of them lasting 30 min. Experimentally, both in the laboratory test bench [9] and in the tests carried out on the full-scale model, it has been seen that this time is sufficient to raise the peak value, i.e., to reach the maximum value where the fiber temperature stabilizes. The sequence is the following:

1. First of all, the temperature is measured without any alteration, neither by heating the hybrid cable, nor by simulating a leak. This allows us to have some initial conditions of the state of the soil. (30 min)
2. The fiber is heated for 30 min.
3. The fiber is allowed to cool for another 30 min.
4. The tap acting on the target area of the leak simulation is opened for 30 min, while monitoring continues.
5. The fiber is heated for 30 min with the tap running.
6. The fiber is allowed to cool for another 30 min with the tap running.
7. The tap is closed and measured for another 30 min.
8. The fiber is heated for 30 min.
9. The fiber is allowed to cool for another 30 min.

Steps 1 to 3 allows us to obtain a reference temperature value and, under these conditions, to observe the thermal rise that can be reached along the fiber without leakage.

Steps 4 to 6 reproduce the effect of the leakage both in the unexcited temperature and the increment obtained during the heating and cooling of the same.

Finally, steps 7, 8, and 9 allow us to see the effect of a wetted zone after leakage on the detection system.

## 3. Results

This section describes the results obtained in different tests. Although the number of tests has been greater, some representative results are shown here. In all the tests, results similar to those detailed below have been obtained. The raw results of the measurements have been included as Supplementary Materials.

Figure 11 shows the thermogram in absolute values of the complete measurement process, as detailed in the previous section. The thermograms show, in abscissae, the different reading points distributed along the fiber, which are indicated according to the distance to the interrogator. The ambient temperature during the test ranged from 10 to 18 °C without rainfall, data extracted from the State Meteorological Agency (Agencia Estatal de Meteorología, AEMET).

Figure 11 shows, according to the Y-axis on the left, that the measurement process began at approximately 9:30 a.m. From that moment on, changes in the measurement cycle can be detected every 30 min, following the steps indicated in the previous section.

This information in absolute values, although it provides interesting data, makes it difficult to visualize the thermal behavior of the fiber. Therefore, the initial measurement value was taken as a reference, and subsequently, the increments and thermal increments along the hybrid cable were used.

The interrogator used is a laboratory instrument. The objective of the work is not to obtain a precise measurement of the temperature along the cable, but rather to measure its temperature variations, mainly those due to excitation by the heating system. For this reason, the temperature values prior to the simulation of a leakage situation are taken as a

reference, these being 0 °C increases. From these, the increases in the heating processes and thermal excitation of the hybrid FO are obtained.

On the other hand, to improve the incremental resolution, the first and last cable sections will be eliminated, since they are not located under the geotextile, but are the sections that carry the cable inside the control house, with a length of about 10 m inside the control house that serves as a reference to detect possible undesired operation of the system.

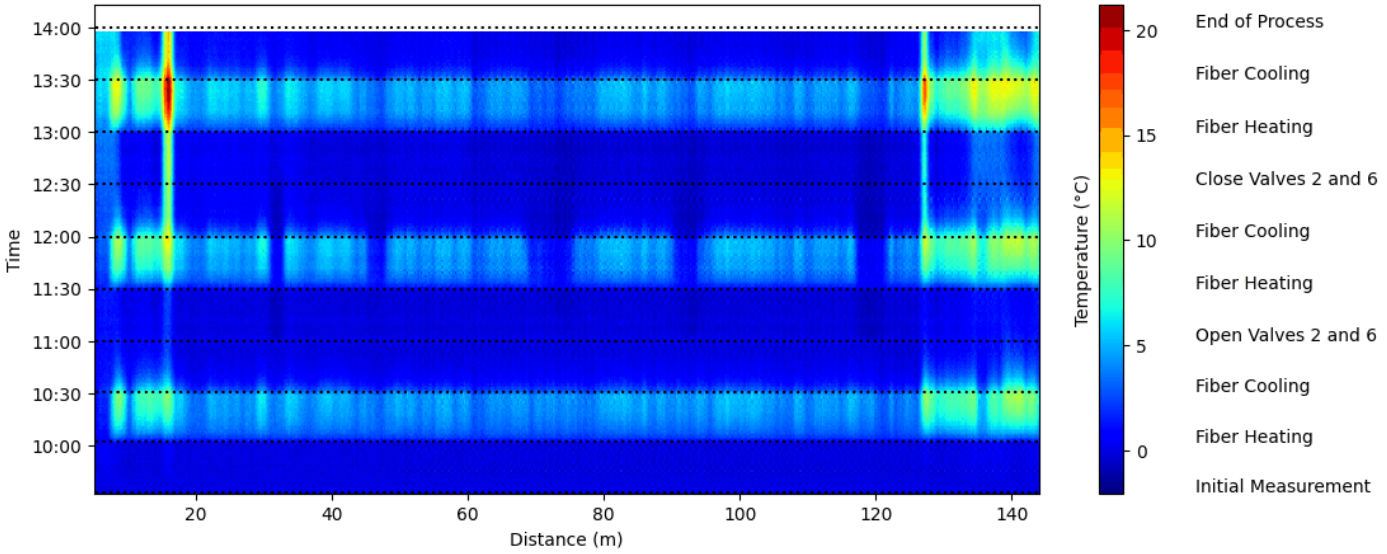


**Figure 11.** Measurements during the detection process along the entire length of the hybrid cable.

Figure 12a shows the plan presented in Figure 2 in detail. The areas that, as a starting hypothesis, are expected to be affected by the simulated leaks when valves #2 and #6 are activated are highlighted in red.

This assumption regarding water flow is based on the construction design, whereby the drainage pipes should collect any water flowing beneath the surface of the geomembrane due to both the capillary action of the soil and gravity. It is also assumed that the water will flow towards the drainage system via the shortest route, although this may not necessarily be the case in reality.

Focusing on the area of interest, i.e., the optical fiber under the water layer between meters 20 and 125 approximately, the thermal increments are more clearly visible, as shown in Figure 12b, which corresponds to the data presented in Figure 11.

The detail shown in Figure 12a allows us to observe the possible affected area. If we look at the position of tap two and the nearest drain, we can see that the area affected by the leak will be around meter 114 of the fiber, even wetting the area near meter 87.

However, from valve #6, which is located on the slope, the water will flow to the upper drain in the plan. This is reflected in Figure 12b, where we observe the thermal increment obtained between 20–30 m, 43 m, 70–75 m, and 90 m, and these zones have correspondence with the water flow and the surrounding wetted areas.

By representing the same test temporarily, the representation shown in Figure 13 is obtained. It shows the thermal increments with respect to time at three specific points on the hybrid cable. These points correspond to tap #2 (Figure 13a), in an area affected by the leakage simulation, meters 92 and 120, orange and green, respectively. In addition, a point, meter 100, unaffected by the leak, is taken as a reference. The graph also highlights in orange the heating periods and in blue the moments when the valves are open to simulate the leak.

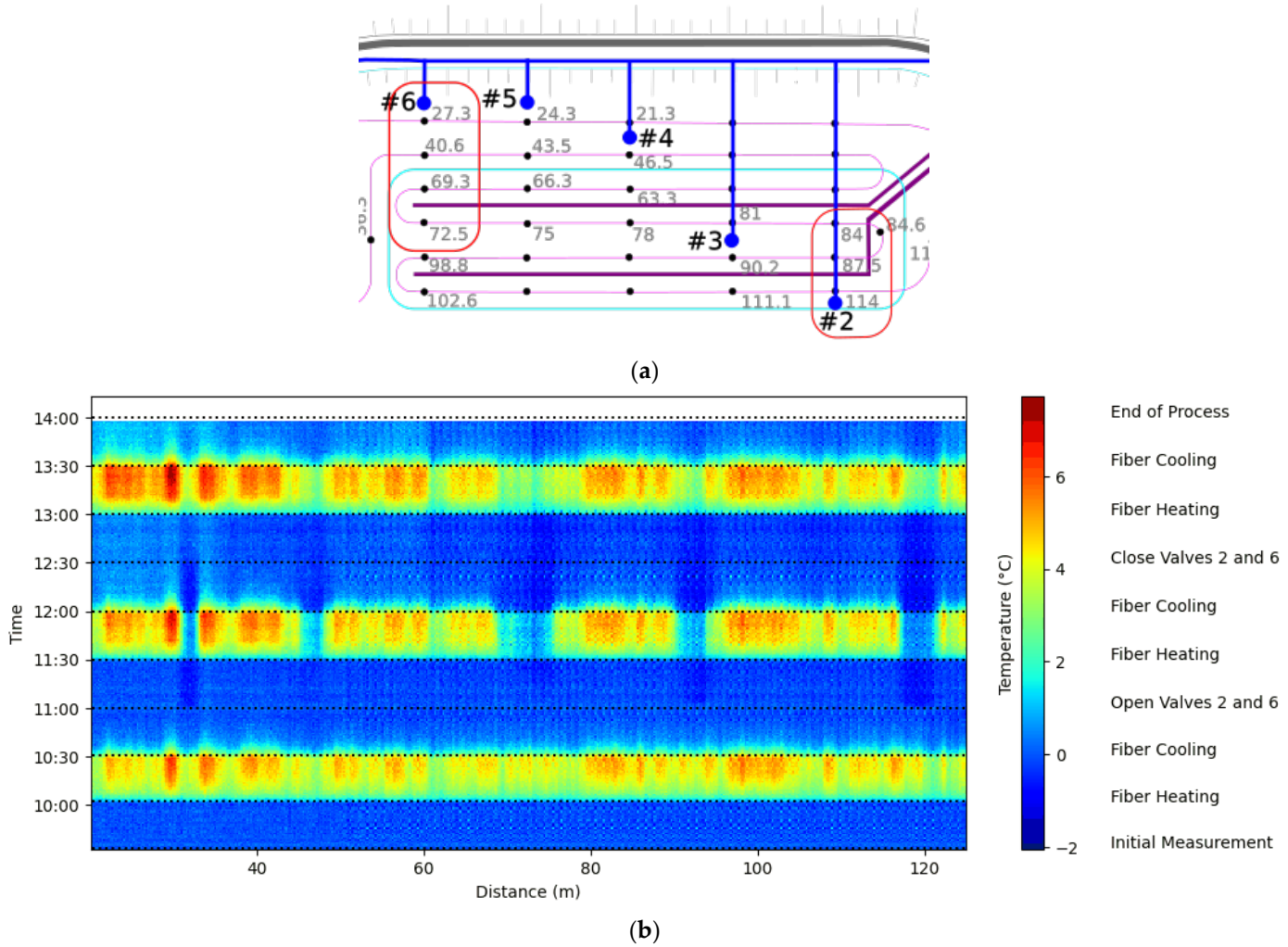


**Figure 12.** (**a**) Detail of Figure 2 highlighting the area expected to be affected by a simulated leak in valves #2 and #6. (**b**) Measurements of the area of interest with ambient temperature between 10 and 18 °C, without precipitation simulating leaks in valves #2 and #6 The valve number is abbreviated as #.

For the zone affected by valve #6, Figure 13b, the metric points selected for the representation are meter 32 (orange) and meter 47 (green); meter 100 again, as a reference, is not affected by the leakage simulation.

Analyzing the results of Figure 13a, it is possible to observe that, in the first heating, the thermal increments in each of the metric points are different and are between 3 and 5 Celsius degrees. This different behavior between points is due to the different height positions of the control points considered, such that those located lower reflect a lower temperature increase as they have a greater height of water column capable of dissipating the heat generated by the thermal pulse. It is also possible to highlight how activating the tap produces a negative increment in the absence of thermal pulse.

Then, with existing water flow, it is observed that the application of the thermal pulse at the reference control point remains the same, while at the points affected by the water flow, the increment achieved is lower, two to three degrees lower, which is consistent with what was expected.

Finally, in the third pulse with the valves closed and the soil under the basin humidified, it can be seen how the heating increment is again higher than with flow, without reaching the levels before the leak, allowing us to discern that the area is humidified. The 100 m reference point maintains its behavior as in the previous steps.

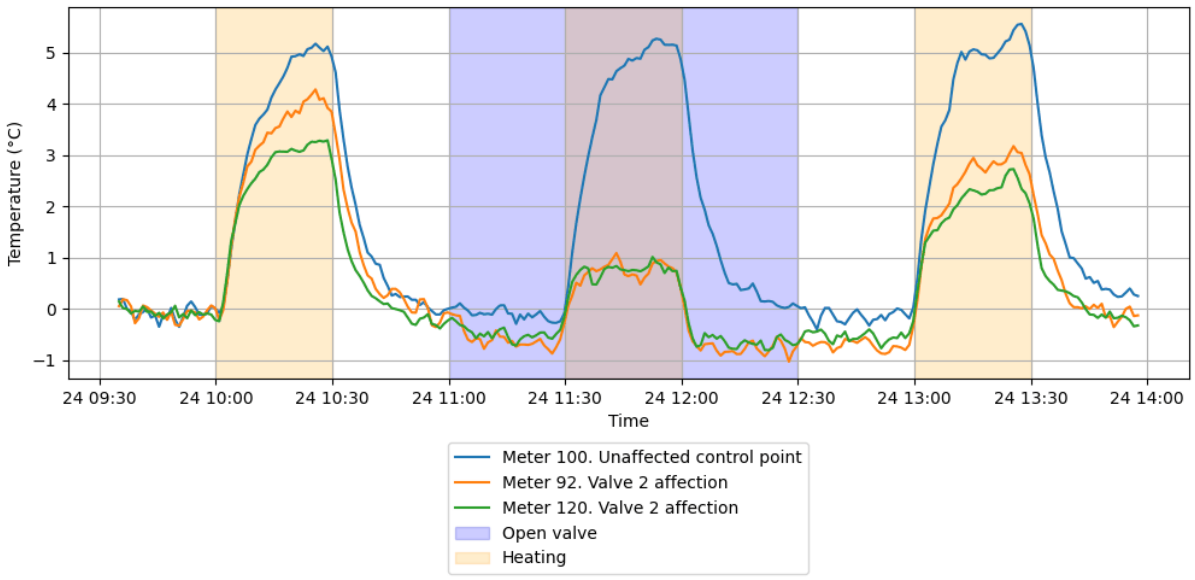


(**a**)

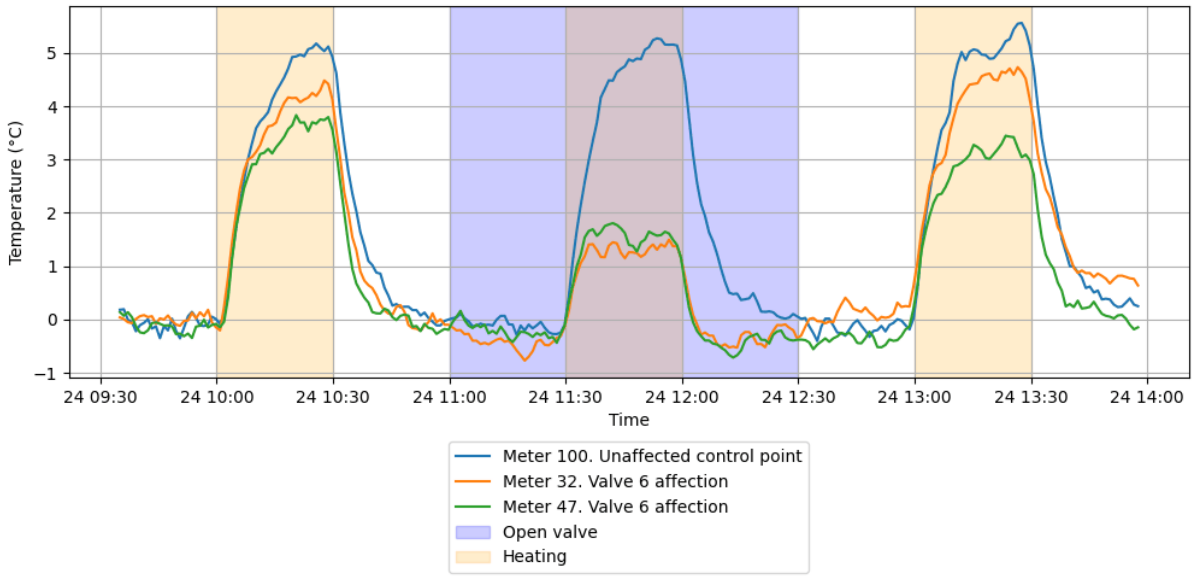


(**b**)

**Figure 13.** Representation of the time evolution of a test: (**a**) zone affected by valve #2; (**b**) zone affected by valve #6.

In Figure 13b, the behavior is similar to that described in Figure 13a for the metric points selected for the representation.

Doing a different analysis, studying the maximum values achieved in the thermal pulses, peak values along the fiber, the graph in Figure 14 is obtained.

The above graph shows how the heating with the valves open is significantly lower, due to the thermal dissipation capacity of the water.

Table 1 summarizes the temperature increases in the different steps described in Section 2.4 for different points along the fiber. The table includes the times that the system remains in each of the states related to the graph in Figure 12b.

We can see that during stable periods, temperature increases are below half a degree. On the other hand, in general, heating pulses achieve increases above one degree when there is no leak simulation, step 2. Whereas with thermal pulse and leak simulation, step 6, the thermal increases obtained are below one degree, the metric reference point reaches a temperature increase of more than 4 °C.

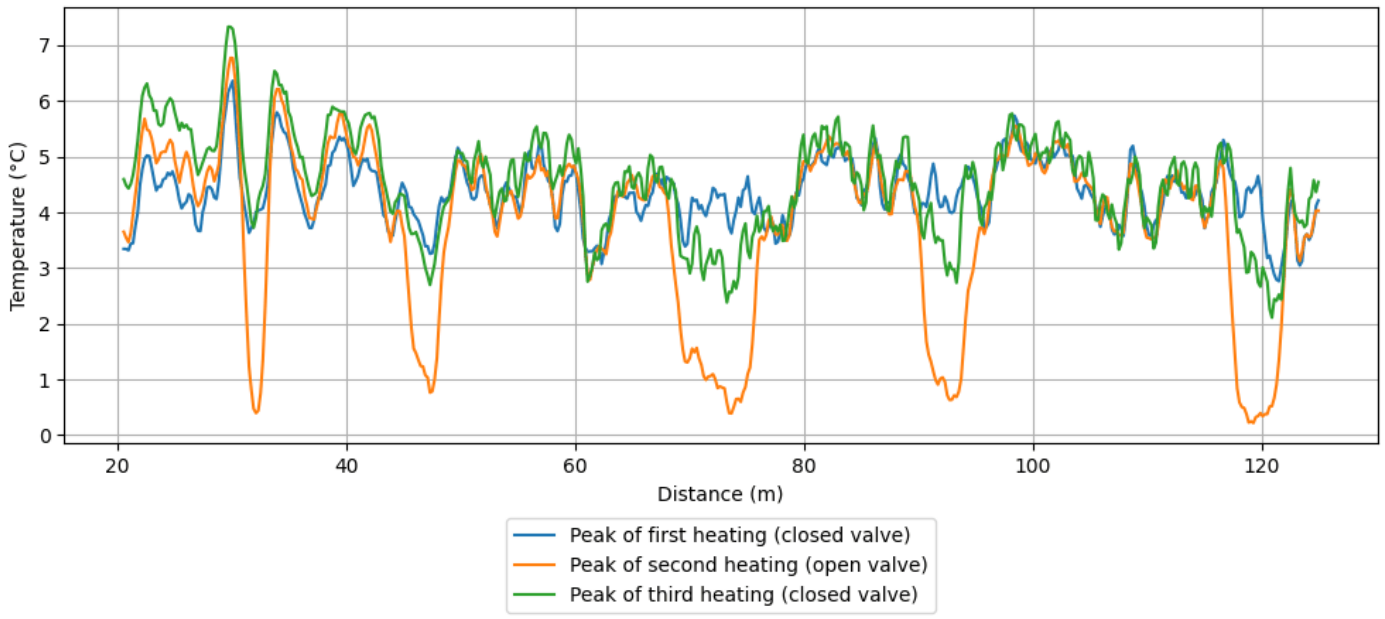


**Figure 14.** Peak values obtained in the three heatings along the fiber during a simulated leak in valves #2 and #6.

**Table 1.** Summary table of maximum temperature increases (°C) reached in the steps described in Section 2.4 for leakage simulation on valves #2 and #6. The valve number is abbreviated as #.

| Meter/Affection Valve # | Stabilization Step 1 | Heating Step 2 | Cooling Step 3 | Stabilization Step 4 | Heating Step 5 | Cooling Step 6 | Stabilization Step 7 | Heating Step 8 | Cooling Step 9 |
|---|---|---|---|---|---|---|---|---|---|
| 100/Unaffected Control Point | −0.18 | 5.01 | −4.62 | 0.12 | 4.43 | −4.41 | 0.01 | 4.56 | −4.45 |
| 32/#6 | −0.19 | 4.34 | −3.65 | 0.02 | 0.99 | −1.16 | 0.92 | 3.05 | −3.08 |
| 47/#6 | −0.22 | 3.71 | −3.33 | −0.06 | 0.83 | −1.05 | 0.58 | 2.35 | −2.87 |
| 92/#2 | −0.04 | 4.07 | −3.47 | −0.19 | 0.36 | −0.75 | 0.23 | 2.48 | −2.35 |
| 120/#2 | −0.36 | 3.18 | −2.75 | 0.01 | 0.19 | −0.85 | 0.36 | 1.74 | −2.09 |
| Time Range | 09:30 10:00 | 10:00 10:30 | 10:30 11:00 | 11:00 11:30 | 11:30 12:00 | 12:00 12:30 | 12:30 13:00 | 13:00 13:30 | 13:30 14:00 |

When the leak disappears, even with the soil moistened by the previous leak simulation, during heating, step 8, temperature increases of more than 1.75 °C are again achieved at the different metric points of the fiber taken for data representation.

A second test performed the day after the one shown in the previous results is shown below. This second test on consecutive days demonstrates the feasibility of using the system in the event of a leak after repairing a previous leak. Figure 15a shows in detail the area near tap #7, highlighting in red the area expected to be affected by a simulated leak at this point under the same conditions as indicated above. Figure 15b shows the thermal increments obtained in the area of interest, with a temperature that ranged from 14 °C at the start of the trial and down to 9 °C, plus there was precipitation from 11 am to 14 am ranging from 0.2 L/m$^2$ to 1.8 L/m$^2$. In this case, the leakage is simulated at valve #7.

Figure 16 shows the time evolution of four metric points, the control point at meter 60 (blue) not affected by the simulation. The points at meter 32 (orange) and 47 (green) are close to the leakage zone, while meter 105 (red) is within the clear zone of leakage action.

The behavior of the control zone is similar in the three thermal pulses, while in meter 32, a higher temperature increase is achieved, this is due to the fact that this zone is outside the water cover, attached to the impermeable sheet. In meter 47, there is hardly any difference with the control measurements, while in meter 107 with water flow, the thermal increment achieved in the put is 1 °C, whereas at the beginning it was 4.5 °C.

Finally, without leakage simulation, the thermal pulse obtains an increment of 3 °C. The detection could be satisfactorily performed.

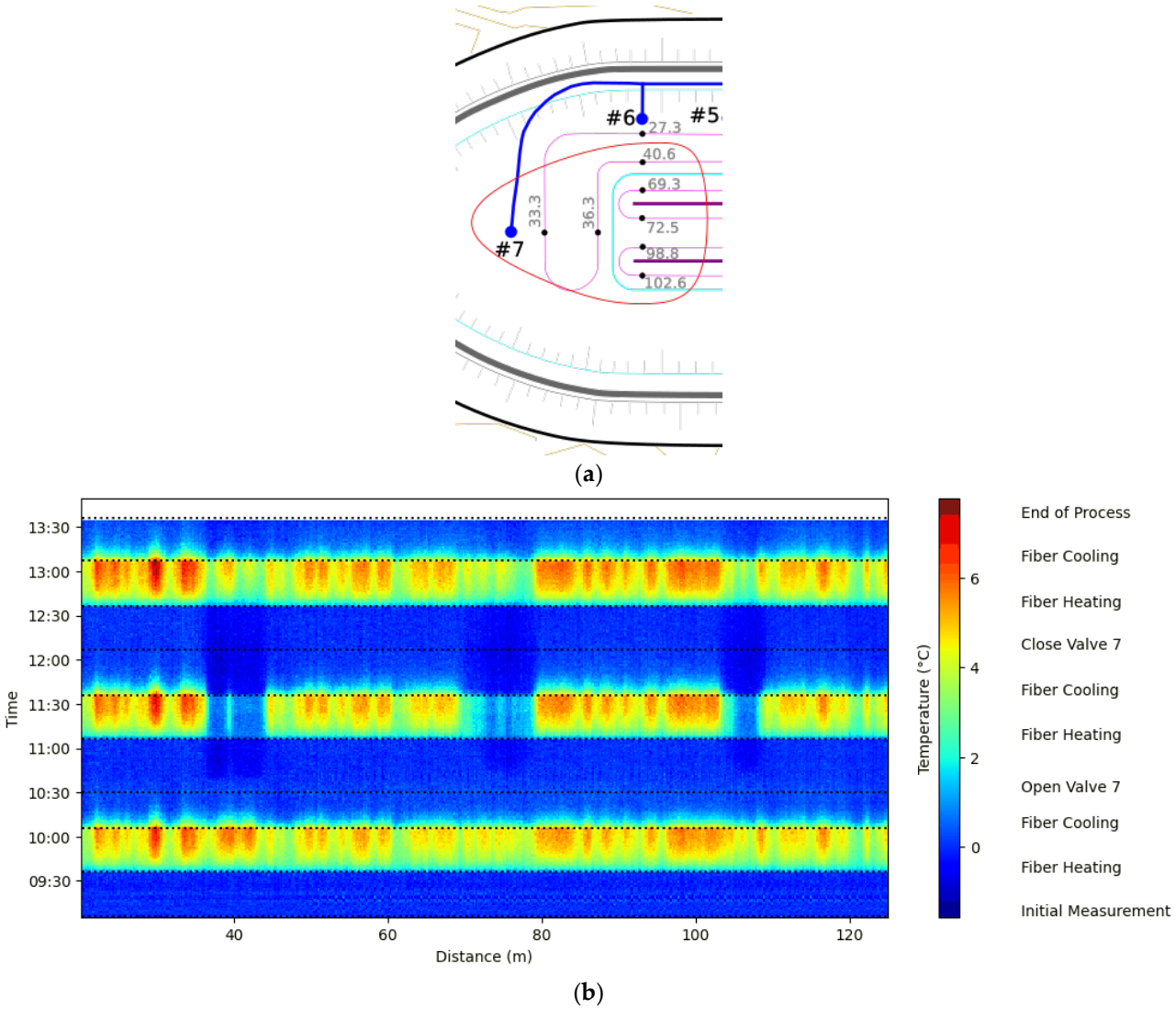


**Figure 15.** (**a**) Detail of Figure 2 highlighting the area expected to be affected by a simulated leak in valves #7. (**b**) Measurements of the area of interest with ambient temperature between 14 and 9 °C, with precipitation simulating leaks in valve #7. The valve number is abbreviated as #.As in the previous case, the thermogram allows us to have an overview of the thermal behavior of the detection system along the entire length of the fiber. In it, we can see that between 38 and 45 m, 70 and 80 m, and 110 and 115 m, the thermal increment is lower with the effect of the valve open in the areas where the water flows to the drains, coinciding with what is observed in the plan of Figure 2.

As in the previous case, the increases obtained for the steps described in Section 2.4 are analyzed again for different points of the fiber. These values are shown in Table 2. The table includes the times that the system remains in each of the states related to the graph in Figure 15b.

The results are consistent with those presented in the previous case. The temperature increases achieved during heating without leakage (step 2) are above three degrees. Meanwhile, in the event of leakage, the increase in the areas affected by the leakage during the thermal pulse (step 5) only reaches a temperature increase of around one degree. Again, in the absence of leakage with the soil moistened after the simulation, it can be seen that the capacity to increase the temperature is around 3 degrees (step 8).

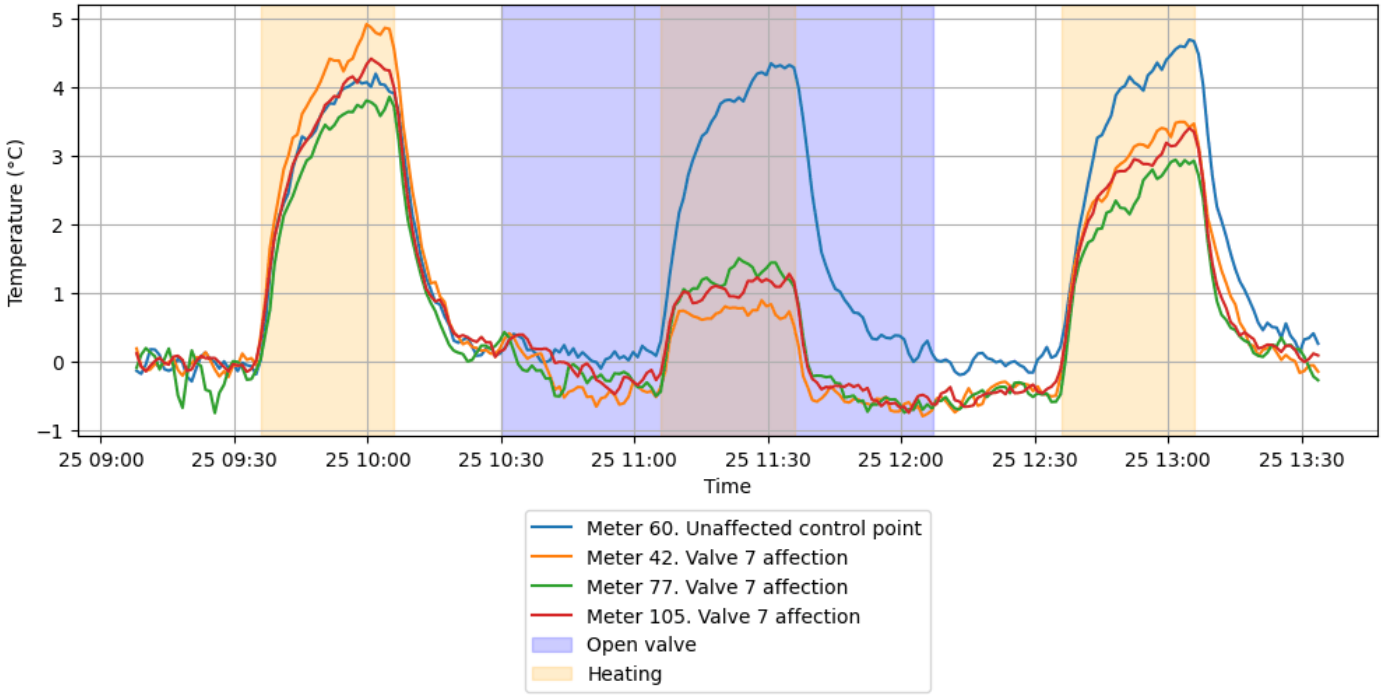


**Figure 16.** Representation of the time evolution of a test, zone affected by valve #7.

Analyzing again the behavior of the system with the heating peaks in the three pulses shown in Figure 17, it is observed how the thermal increments under the effect of the leakage simulation are clearly lower in the zones of action of the water flow.

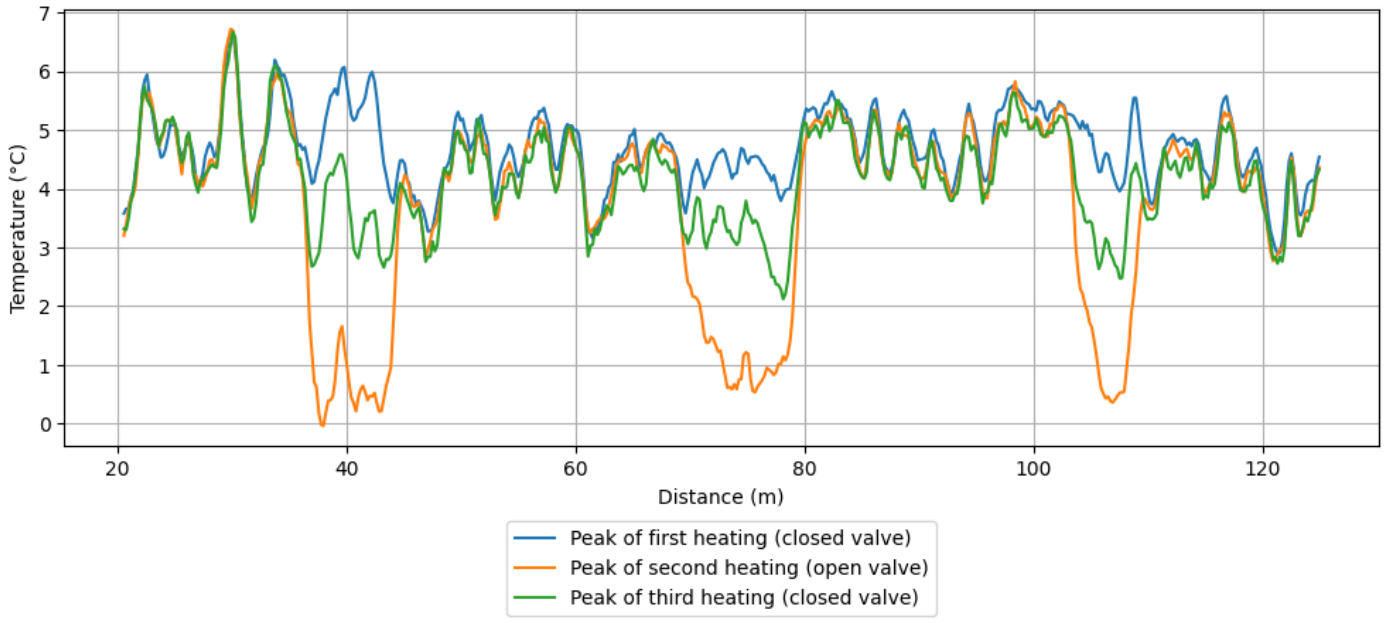


**Figure 17.** Peak values obtained in the three heatings along the fiber during a simulated leak in valve #7.

These results allow us to validate the performance of the leak detection system to establish the location of the leak with a heating power of 7.5 W/m.

**Table 2.** Summary table of maximum temperature increases (°C) reached in the steps described in Section 2.4 for leakage simulation on valve #7. The valve number is abbreviated as #.

| Meter/Affection Valve # | Stabilization Step 1 | Heating Step 2 | Cooling Step 3 | Stabilization Step 4 | Heating Step 5 | Cooling Step 6 | Stabilization Step 7 | Heating Step 8 | Cooling Step 9 |
|---|---|---|---|---|---|---|---|---|---|
| 60/Unaffected Control Point | 0.16 | 3.37 | −3.53 | 0.1 | 3.54 | −3.87 | 0.2 | 4.11 | −4.22 |
| 42/#7 | 0.19 | 3.66 | −3.91 | −0.7 | 0.66 | −0.95 | 0.32 | 3.22 | −3.3 |
| 77/#7 | 0.13 | 3.33 | −2.93 | −0.87 | 1.1 | −1.52 | 0.09 | 2.94 | −2.99 |
| 105/#7 | 0.2 | 3.18 | −3.42 | −0.35 | 1.01 | −1.39 | 0.51 | 3.05 | −3.01 |
| Time Range | 09:00<br>09:36 | 09:36<br>10:06 | 10:06<br>10:30 | 10:30<br>11:06 | 11:06<br>11:36 | 11:36<br>12:07 | 12:07<br>12:36 | 12:36<br>13:06 | 13:06<br>14:00 |

## 4. Discussion

Subsurface monitoring systems based on DTS using hybrid fiber optics with Raman effect interrogators for monitoring water detection in hydraulic infrastructures enable both the detection and localization of leaks in these infrastructures.

The application of this technique requires a study of the specific type of hydraulic infrastructure to which it is to be applied. For this reason, passive monitoring systems can be found, i.e., those that do not produce external excitation or heating of the fiber, but rather perform a distributed measurement of the temperature along the length of the fiber over time, similar to the measurement recorded by a weather station at a single point in space.

In contrast to these passive systems, there are active systems, which use a thermal pulse to modify the hybrid temperature and allow the measurement, in addition to the temperature along the fiber of the thermal dissipation along the fiber produced by interaction with the environment, the response to which will not be solely dependent on the natural temperature conditions in the subsoil.

In [11–13], the authors monitored a river dam to assess the behavior of water in the dam body under flood conditions, work that they have carried out for years, developing the project and whose study has given rise to the aforementioned publications. These publications collect measurements taken during the four seasons of the year, observing different river floods. During these floods, the thermal variation of the hybrid fiber optic cable was around 2 °C with a passive monitoring system. The monitoring system is not based solely on DTS measurement with fiber optics, but also relies on sensors from other technologies. For distributed temperature monitoring, they use an Oryx SR DTS interrogator, capable of 2 m spatial resolution and 0.1 °C temperature resolution for 2 km.

Focusing on systems that use active measurement, we find [14], where the aim is to perform distributed temperature measurement to determine the specific flow rate of groundwater under a branched river. To do this, approximately 100 m of hybrid fiber optic cable is laid under the river at a depth of approximately 5 m. The interrogator is a Silixa XT-DTS with a resolution of 0.01 °C and a spatial resolution of 0.25 m. To measure the thermal increment, an electrical pulse with a power of 15 W/m is applied to the cable for 1 h. After this time, the cable is left to cool for approximately another hour. Under these conditions, the thermal increase obtained is approximately 5 °C.

For their part, ref. [17] uses this technique to estimate infiltration rates in a managed aquifer recharge framework. In their model, they use about 50 m of hybrid cable, to which they only apply the thermal pulse at 7.5 m. They use a hybrid system for detection, which is both passive and active at the same time. The interrogator used is a DTSN4386B with a resolution of 25 cm. They apply a thermal pulse of 17.98 W/m for 9.5 h.

Another active and passive measurement system is presented in [15], which uses the same interrogator as in [14] (Silixa XT-DTS with a resolution of 0.01 °C and a spatial resolution of 0.25 m) with a structure similar to [17]. However, 150 m of cable is laid for the measurement, buried under the stream, and 60 m of this is connected to allow it to be heated

by a thermal pulse. The thermal pulse applied is 35 W/m for 4 h, with monitoring during the 3 h following heating to see how the cable cools down. Under these conditions, thermal increases ranging from 19 °C to 36 °C are obtained after 3 h and 45 min of pulse. The objective of this project is to locate and quantify the variability of groundwater discharge in a headwater stream.

In [5], a system similar to the one described in this paper was implemented, whereby an active DTS system was installed for dam auscultation. In this system, 2369 m were distributed with a thermal pulse excitation power of 0.732 W/m, achieving thermal increases of 0.5 °C in the dam body with an excitation time of 30 min.

In this study, the active DTS monitoring system with FO based on the Raman effect has been adapted to the construction conditions of the ponds, and measurement procedures have been established and validated based on the results of the laboratory work presented in [9]. The measurement conditions tested in the prototype raft for a cable length of 150 m, applying a thermal pulse of 7.5 W/m for 30 min, yielded thermal increases of 4.5 °C in the absence of leakage, 1.5 °C with leakage, and 3.5 °C after stopping the leakage simulation with the soil moistened.

The results obtained validate the proposed development with the established excitation power, and the pulse times allow us to distinguish between dry, wet, and saturated soil conditions. Furthermore, increasing both the power and the excitation time could increase the thermal increments achieved, thereby increasing the detection capacity.

The determination of the absolute values of the thermal increments recorded along the optical fiber is influenced by heat dissipation processes, which affect the behavior and temperature increase obtained during the thermal pulse. This behavior is due to both thermal conduction (which in turn depends on the moisture conditions of the subsoil) and advection in the event that there is a flow of water that allows a greater amount of heat caused by the thermal flow to be evacuated.

In addition, increasing the excitation power or duration may enhance thermal increments and consequently improve detection sensitivity.

## 5. Conclusions

The results obtained from the scale model of the leak detection system have made it possible to verify the operating conditions of this type of monitoring system for its implementation in ponds, with the aim of identifying and locating possible leaks during their useful life.

Leaks in hydraulic infrastructures, except in catastrophic situations involving a serious structural failure, are slow processes in all other cases, so their surveillance requires continuous monitoring in order to detect them accurately and at an early stage.

The proposed system allows us, by means of distributed temperature measurement (DTS) and the application of a thermal pulse, to generate and detect a thermal increment intense enough to be able to determine the location of a leak in a pond due to the change of thermal behavior in the optical fiber, a change due to the alteration of the hydraulic conditions of the soil.

The tests performed have made it possible to record the thermal increments along the optical fiber deployed in different environmental conditions and in a real prototype pond.

The temperature increases recorded showed significant differences between areas not affected by a simulated leak event, reaching temperature increases of 5 °C, while during the same test, the temperature at points affected by a simulated leak increased by 1 °C when an electrical pulse of 7.5 W/m was applied. These tests have validated the technology for use in a real-life situation. Leakage from the waterproofing sheet can be identified by the thermal increment.

This research contributes directly to the advancement of the agricultural sector towards agriculture and livestock farming 4.0. This innovative low-cost monitoring technology contributes to digital and environmental transformation, a sector in which instrumentation and digital technologies are still a pending subject. Moreover, in the specific case of irrigation water storage ponds, leak detection is an improvement in the management of the planet's water resources, while in a slurry storage pond, early detection of leaks is a fundamental advance in environmental conservation, especially to preserve the good condition of the receiving media, especially the hydrogeological environment.

**Supplementary Materials:** The following supporting information can be downloaded at https://www.mdpi.com/article/10.3390/app16010465/s1; Raw data from the measurements presented in the article.

**Author Contributions:** Conceptualization, D.A.-C., P.L.L.-J., J.P., Ó.M., A.A.-O. and B.R.; methodology, D.A.-C. and Ó.M.; validation, D.A.-C. and P.L.L.-J.; formal analysis, D.A.-C. and P.L.L.-J.; data curation, J.P.; writing—original draft preparation, D.A.-C. and P.L.L.-J.; writing—review and editing, Ó.M. and B.R.; project administration, A.A.-O. and B.R.; funding acquisition, A.A.-O. and B.R. All authors have read and agreed to the published version of the manuscript.

**Funding:** This project has been funded by the Aid Programme for innovative business clusters in the 2022b call of the Ministry of Industry, Trade and Tourism, with exp. no. AEI-010500-2022b-320 and with the consortium formed by Asoc. Cluster para el Uso Eficiente del Agua (ZINNAE), Canteras de Ejea S.L., Ingeniería de Obras de Zaragoza S.L. and Escuela Universitaria Politécnica de la Almunia.

**Institutional Review Board Statement:** Not applicable.

**Informed Consent Statement:** Not applicable.

**Data Availability Statement:** The original data presented in the study are openly available in Zenodo at doi:10.5281/zenodo.17957174.

**Acknowledgments:** The authors would like to thank the Tecnalia Research & Innovation Foundation for their support for this project.

**Conflicts of Interest:** Author Óscar Muñoz was employed by the company "Smart Systems, Tecnalia, Basque Research and Technology Alliance (BRTA)". The remaining authors declare that the research was conducted in the absence of any commercial or financial relationships that could be construed as a potential conflict of interest.

## Abbreviations

The following abbreviations are used in this manuscript:

| | |
|---|---|
| FO | Fiber Optic |
| DTS | Distributed Temperature Sensor |
| AEMET | Agencia Estatal de Meteorología, State Meteorological Agency |
| PET | Polyethylene Terephthalate |
| HDPE | High-Density Polyethylene |
| RMS | Root Mean Square |

## References

1. Implementing Decision—2017/302—EN—EUR-Lex. Available online: https://eur-lex.europa.eu/eli/dec_impl/2017/302/oj/eng (accessed on 2 June 2025).
2. Schenato, L. A Review of Distributed Fiber Optic Sensors for Geo-Hydrological Applications. *Appl. Sci.* **2017**, *7*, 896. [CrossRef]
3. Leng, Y.B.; Zhu, P.; Zhou, Y. Monitoring Technology for Embankment Dam Safety Based on Distributed Optical Fiber Sensing and Its Prospect. *Prog. Geophys.* **2007**, *22*, 1001–1005.
4. Ukil, A.; Braendle, H.; Krippner, P. Distributed Temperature Sensing: Review of Technology and Applications. *IEEE Sens. J.* **2012**, *12*, 885–892. [CrossRef]

5. Sanchez, J.C.; Muñoz, O.; Russo, B.; Oliete, A.A.; Paindelli, A. Distributed temperature sensors system. Field tests on earth dam. *DYNA* **2023**, *98*, 163–168. [CrossRef] [PubMed]
6. Cai, D.; Xiao, H. Discussion on Mechanism of Distributed Fiber Optical Leakage Monitoring Technology Based on Temperature Measurement. *Rock Soil Mech.* **2008**, *29*, 550–554.
7. Bekele, B.; Song, C.; Abualshar, B.; Hunde, A. Real-Time Seepage Health Monitoring Using Spatial Autocorrelation of Distributed Temperature Data from Fiber Optic Sensor. *J. Civ. Struct. Health Monit.* **2025**, *15*, 1101–1116. [CrossRef]
8. Kang, W. Understanding Seepage in Levees and Exploring the Applicability of Using an Optical-Fiber Distributed Temperature System and Smoothing Technique as a Monitoring Method. *Sensors* **2023**, *23*, 4780. [CrossRef] [PubMed]
9. Antolín Cañada, D.; López Julián, P.L.; Pérez Esteras, J.; Sánchez Catalán, J.C.; Acero Oliete, A.; Russo, B. Desarrollo en laboratorio de un sistema de detección temprana de fugas en balsas mediante tecnología de fibra óptica. *Ing. Del Agua* **2023**, *27*, 211–221. [CrossRef]
10. Ghafoori, Y.; Vidmar, A.; Říha, J.; Kryžanowski, A. A Review of Measurement Calibration and Interpretation for Seepage Monitoring by Optical Fiber Distributed Temperature Sensors. *Sensors* **2020**, *20*, 5696. [CrossRef] [PubMed]
11. Fabbian, N.; Simonini, P.; De Polo, F.; Schenato, L.; Cola, S. Temperature Monitoring in Levees for Detection of Seepage. *Bull Eng. Geol. Environ.* **2024**, *83*, 69. [CrossRef]
12. Fabbian, N.; Cola, S.; Simonini, P.; De Polo, F.; Schenato, L.; Tedesco, G.; Marcato, G.; Dalla Santa, G. Innovative and Traditional Monitoring System for Characterizing the Seepage inside River Embankments along the Adige River in Salorno (Italy). In Proceedings of the International Society for Soil Mechanics and Geotechnical Engineering, London, UK, 5–9 September 2022.
13. Cola, S.; Girardi, V.; Bersan, S.; Simonini, P.; Schenato, L.; De Polo, F. An Optical Fiber-Based Monitoring System to Study the Seepage Flow below the Landside Toe of a River Levee. *J. Civ. Struct. Health Monit.* **2021**, *11*, 691–705. [CrossRef]
14. Sai Louie, A.J.; Morgan, L.K.; Banks, E.W.; Dempsey, D.; Wilson, S. Testing the Reproducibility of Active-Distributed Temperature Sensing for Measuring Groundwater Specific Discharge beneath a Braided River. *J. Hydrol.* **2024**, *633*, 130877. [CrossRef]
15. Simon, N.; Bour, O.; Faucheux, M.; Lavenant, N.; Le Lay, H.; Fovet, O.; Thomas, Z.; Longuevergne, L. Combining Passive and Active Distributed Temperature Sensing Measurements to Locate and Quantify Groundwater Discharge Variability into a Headwater Stream. *Hydrol. Earth Syst. Sci.* **2022**, *26*, 1459–1479. [CrossRef]
16. Bense, V.F.; Read, T.; Bour, O.; Le Borgne, T.; Coleman, T.; Krause, S.; Chalari, A.; Mondanos, M.; Ciocca, F.; Selker, J.S. Distributed Temperature Sensing as a Downhole Tool in Hydrogeology. *Water Resour. Res.* **2016**, *52*, 9259–9273. [CrossRef]
17. Glaude, R.; Simon, N.; Brouyère, S. Innovative Use of Passive and Active Distributed Temperature Sensing for Estimating Infiltration Rates in a Managed Aquifer Recharge Framework. *J. Hydrol.* **2025**, *662*, 133848. [CrossRef]
18. Radzicki, K.; Stoliński, M. Seepage Monitoring and Leaks Detection along an Earth Dam with a Multi-Sensor Thermal-Active System. *Bull. Eng. Geol. Environ.* **2024**, *83*, 362. [CrossRef]
19. Gil-Rodríguez, M.; Rodríguez-Sinobas, L.; Benítez-Buelga, J.; Sánchez-Calvo, R. Application of Active Heat Pulse Method with Fiber Optic Temperature Sensing for Estimation of Wetting Bulbs and Water Distribution in Drip Emitters. *Agric. Water Manag.* **2013**, *120*, 72–78. [CrossRef]
20. Yao, J.-C.; Shi, B.; Liu, J.; Sun, M.-Y.; Fang, K.; Yao, J.; Gu, K.; Zhang, W.; Zhang, J.-W. Improvement and Performance Evaluation of a Dual-Probe Heat Pulse Distributed Temperature Sensing Method Used for Soil Moisture Estimation. *Sensors* **2022**, *22*, 7592. [CrossRef] [PubMed]
21. Su, H.; Cui, S.; Wen, Z.; Xie, W. Experimental Study on Distributed Optical Fiber Heated-Based Seepage Behavior Identification in Hydraulic Engineering. *Heat Mass Transf.* **2019**, *55*, 421–432. [CrossRef]